



Full Text View

[Volume 30, Issue 5 \(May 2000\)](#)

Journal of Physical Oceanography

Article: pp. 1069–1082 | [Abstract](#) | [PDF \(664K\)](#)

Seasonal and Interannual Variability in a Model of the Mediterranean under Derived Flux Forcing

Paul G. Myers and Keith Haines

Department of Meteorology, University of Edinburgh, Edinburgh, United Kingdom

(Manuscript received August 17, 1998, in final form June 16, 1999)

DOI: 10.1175/1520-0485(2000)030<1069:SAIVIA>2.0.CO;2

ABSTRACT

A 100-yr integration of a Mediterranean Sea model is performed with surface restoring to monthly varying T , S , followed by 100 years of integration with surface fluxes of heat and freshwater alone. The fluxes are diagnosed from the restoring boundary run and are shown to agree favorably with the observations. The model properties remain stable under flux forcing, reproducing all major water masses and a realistic thermohaline circulation, although with more variability than the restoring run. Annual average production of Levantine Intermediate Water (LIW) is 1.3 ± 0.3 Sv on a core density of $\sigma_\theta = 29.05$. A major component of variation is on a timescale of 2–3 yr and is correlated with changes in surface salinity in the Levantine by 0.1 psu, which are in turn related to a variable path for the modified Atlantic water in the eastern basin. Smaller variations in production of deep waters in the Adriatic and Western Mediterranean are also found to be significantly correlated with the LIW production at lags of 2 and 6 yr respectively.

1. Introduction


The Mediterranean ([Fig. 1](#) ) is governed by a large scale anti-estuarine buoyancy-driven circulation. Inflowing Atlantic water, continually modified by excess evaporation [modified Atlantic water (MAW)], flows across the western and eastern basins into the Levantine. Cooling in winter causes convection to intermediate depths mainly in the Rhodes gyre forming Levantine Intermediate Water (LIW). This salty intermediate water returns to the west underneath the MAW, forming the main component of the Mediterranean outflow to the Atlantic ([Kinder and Parrilla 1987](#)). Modeling studies show LIW dispersal paths can be sensitive to the wind ([Myers et al. 1998a](#)), but it is the buoyancy forcing that controls LIW production. Separate deep thermohaline cells also exist in the different subbasins. In the east LIW is exported to the Adriatic (and more recently the

Table of Contents:

- [Introduction](#)
- [Model and spinup](#)
- [Surface fluxes](#)
- [Model behavior under](#)
- [Discussion and summary](#)
- [REFERENCES](#)
- [TABLES](#)
- [FIGURES](#)

Options:

- [Create Reference](#)
- [Email this Article](#)
- [Add to MyArchive](#)
- [Search AMS Glossary](#)

Search CrossRef for:

- [Articles Citing This Article](#)

Search Google Scholar for:

- [Paul G. Myers](#)
- [Keith Haines](#)

Aegean; [Roether et al. 1996](#)), to precondition the system for deep convection and the formation of Eastern Mediterranean Deep Water (EMDW) that sinks and fills the deep eastern basin ([Schlitzer et al. 1991](#)). In the west LIW is transported to the Gulf of Lions, where winter cooling produces Western Mediterranean Deep Water (WMDW), which fills the deep western basin and also contributes to the Gibraltar outflow ([Kinder and Parrilla 1987](#)).

Modeling of the Mediterranean has been going on for the last decade although most studies have focused on the wind-driven circulation. Studies by [Stanev et al. \(1989\)](#) and [Pinardi and Navarra \(1993\)](#) examined the wind-driven general circulation of the Mediterranean, concentrating on forcing at different timescales. The seasonal characteristics of the Mediterranean Sea were simulated by [Roussenov et al. \(1995\)](#) and, except for the poor deep-water renewal, their model reproduced many of the key features of the circulation for the first time. Using the Princeton ocean model, [Zavatarelli and Mellor \(1995\)](#) produced more thermohaline aspects of the real Mediterranean, including the inflow/outflow, LIW path, and some of the deep-water formation. Detailed studies of the western basin highlighted the key role of density gradients at the straits connecting the basins and topography and thermohaline forcing in setting up the circulation ([Herbaut et al. 1996, 1997](#)). In a recent series of papers, [Haines and Wu \(1995\)](#) and [Wu and Haines \(1996, 1998\)](#) modeled the dispersal of LIW throughout the entire Mediterranean. They found that accurate representation and modeling of this water mass was key in reproducing a reasonable basin circulation. [Haines and Wu \(1998\)](#) also found that for a $\frac{1}{4}^\circ$ model proper parameterization of subgrid scale processes [e.g., with the Gent and McWilliams parameterization; [Gent and McWilliams \(1990\)](#), hereafter GM] is necessary to get the EMDW overflow at Otranto and thus we adopt their GM parameters here in [section 2](#). A recent project, the Mediterranean Models Evaluation Experiment (MEDMEX), provided an intercomparison of five models of the Mediterranean ([Beckers et al. 1996, 1997](#)), highlighting some of the differences and similarities.

In all of these studies, except for the short integrations of [Roussenov et al. \(1995\)](#), [Zavatarelli and Mellor \(1995\)](#) and [Herbaut et al. \(1997\)](#), restoring boundary conditions were used at the surface for both temperature and salinity. [Roussenov et al. \(1995\)](#) and [Herbaut et al. \(1997\)](#) both maintain the restoring condition on salinity while directly using heat fluxes (from bulk formulas and a numerical weather prediction model, respectively). [Zavatarelli and Mellor \(1995\)](#) use both heat and freshwater surface fluxes taken from observational climatologies ([May 1982; Jaeger 1976](#)).

For restoring boundary conditions, the surface fluxes are parameterized as simple, linear Newtonian damping conditions,

$$Q_T = -\frac{\rho_0 C_p \Delta z_1}{\tau_T} (T_1(\lambda, \phi, t) - T^*(\lambda, \phi, t)) \quad (1)$$

$$Q_S = -\frac{\rho_0 \Delta z_1}{\tau_S} (S_1(\lambda, \phi, t) - S^*(\lambda, \phi, t)), \quad (2)$$

where $T_1(\lambda, \phi)$ and $S_1(\lambda, \phi)$ are the model's upper ocean box (upper-layer thickness Δz_1 being a constant 10 m in our model) temperature and salinity values, respectively, at longitude λ and latitude ϕ ; C_p is the specific heat at constant pressure, ρ_0 is a reference density, and $\tau_{T,S}$ are restoring timescales ([Haney 1971](#)). Here T^* and S^* are a reference temperature and salinity that the surface tracers are relaxed back toward and can vary seasonally.

For heating the Newtonian damping was originally based on the longwave emission, sensible heating, and latent heat fluxes being dependent on ocean temperature ([Weaver and Hughes 1992](#)), and the decay timescale τ_T is then associated with the lag of sea surface temperature behind the seasonal cycle of insolation ([Barnier et al. 1995](#)). Originally, T^* was defined in terms of the atmospheric temperature ([Haney 1971](#)) but observed sea surface temperatures are more commonly used now.

However, surface freshwater fluxes do not depend on the ocean salinity, with evaporation mainly a function of the air-sea temperature difference and precipitation depending mainly on atmospheric processes. Due to the sparsity of open ocean evaporation and precipitation measurements however ([Weaver and Hughes 1992](#)), this type of boundary condition is often used, with S^* being observed sea surface salinities.

Restoring boundary conditions are advantageous for simulating a steady thermohaline circulation by nudging surface water properties towards well observed values. Slight errors in surface water properties at water formation sites can lead to a weakening or over intense convection and thus a poor simulation of the thermohaline circulation. The use of poorly known air-sea fluxes often cause surface model properties and circulations to drift unacceptably for this reason ([Manabe and Stouffer 1988](#)). However restoring boundary conditions will also damp natural variability in the system and so cannot be used to study the stability of the thermohaline circulation or the sensitivity to small changes in fluxes. These problems are extremely important if we want to learn how the present thermohaline circulation might change in future or how it might have looked in paleoclimate scenarios.

This paper describes a Mediterranean GCM that maintains a good representation of the circulation, including the thermohaline component, using flux forcing alone. The modeling was based on the work of [Haines and Wu \(1995\)](#), [Wu and Haines \(1996, 1998\)](#) and [Myers et al. \(1998a\)](#). [Section 2](#) describes the model spinup. [Section 3](#) describes the diagnosis of the surface fluxes from a surface restoring run of the model and compares them with observations. [Section 4](#) describes the model run with flux forcing alone and discusses the additional variability observed. A summary is provided in [section 5](#).

2. Model and spinup

The model used is the Modular Ocean Model-Array (MOMA), a Bryan–Cox–Semtner type ocean general circulation model (OGCM) using the [Killworth et al. \(1991\)](#) free surface scheme. The revised horizontal and vertical advection schemes of [Webb \(1995\)](#) are used for the baroclinic momentum equation. The tracer advection schemes are modified to include the [Gent and McWilliams \(1990\)](#) eddy parameterization and a flux-limiting scheme ([Stratford 1999](#)) based on the work of [Thuburn \(1996\)](#). The basic model is described in greater detail by [Webb \(1993\)](#) and has been used for the Mediterranean to study changes in the basin's thermohaline circulation, both for the present ([Myers et al. 1998a](#)) and past climates ([Myers et al. 1998b](#)).

Basin resolution is $0.25^\circ \times 0.25^\circ$ with 19 vertical levels (mainly concentrated in the upper part of the water column to resolve the thermocline). The horizontal biharmonic viscosity coefficient is $A_h = 1.5 \times 10^{18} \text{ cm}^4 \text{ s}^{-1}$. The vertical momentum diffusion is $A_v = 1.5 \text{ cm}^2 \text{ s}^{-1}$. The Gent and McWilliams thickness diffusion parameter was $5.0 \times 10^5 \text{ cm}^2 \text{ s}^{-1}$ for the first 40 years of integration and then $2.0 \times 10^5 \text{ cm}^2 \text{ s}^{-1}$ thereafter, and the maximum (reciprocal) slope of isopycnals is 100.0. Convective adjustment is performed using the complete convection scheme of [Rahmstorf \(1993\)](#). To handle the exchanges with the Atlantic, a small box is added outside of Gibraltar, where the temperature and salinity at all depths are relaxed on a 1-day timescale to the climatological values of [Levitus \(1982\)](#).

Wind stress data is obtained from the European Centre for Medium Range Weather Forecasting (ECMWF), based on a 7-yr climatology (1986–92). These data are reanalyzed monthly mean wind stress fields on a $1.125^\circ \times 1.125^\circ$ grid, which have been computed using four times daily analyses.

For the spinup, restoring conditions are applied at the surface for the tracers, using modified monthly T^* , S^* based on the Mediterranean Oceanic Data Base (MODB)—MED5 ([Brasseur et al. 1996](#)). The forcing repeats every year. The relaxation timescale for temperature is 2 h (acting on a top layer of 10 m thickness) while it is 5 days for salinity, except in the Levantine, where it smoothly decreases to 2 h east of 23°E . This choice of surface restoring timescale is based upon the work of [Wu and Haines \(1996\)](#) and produces proper water mass formation by rapid cooling in winter while leaving an active role for salinity advection throughout most of the domain.

The model was integrated with restoring boundary conditions for 100 years, sufficient for the model to have reached equilibrium, including the deep waters which have a renewal timescale of up to 100 years ([Stratford and Williams 1997](#)). Surface flux fields were then diagnosed and are compared with observations below.

3. Surface fluxes

a. Observations

Estimates of air–sea heat fluxes based on bulk formulas still suffer from global uncertainties, particularly in shortwave radiation input (e.g., [Gilman and Garrett 1994](#); [Josey et al. 1999](#)). Fortunately the semienclosed nature of the Mediterranean Sea allows the estimate of heat transport through the Strait of Gibraltar, which would equal the basin mean surface flux under long-term steady-state conditions. The flow through the strait is essentially two-layer with a warm, fresh inflow from the Atlantic above a cool, salty outflow layer. Hydrographic measurements through the strait suggest that the surface equivalent heat transport into the basin falls in the range of $3\text{--}10 \text{ W m}^{-2}$ ([Robinson et al. 1971](#); [Bethoux 1979](#)), with some of the latest measurements suggesting $5.3\text{--}6.2 \text{ W m}^{-2}$ ([Macdonald et al. 1994](#)). Similar measurements at Sicily imply annual surface heat losses for the western and eastern basins, at 5.7 ± 7 and $5.9 \pm 4 \text{ W m}^{-2}$, respectively ([Send et al. 1997](#)). [Artegiani et al. \(1997\)](#) estimated a mean surface heat loss for the Adriatic of $19\text{--}22 \text{ W m}^{-2}$ from atmospheric bulk formulas.

Estimates of $E - P$ may be obtained via either the terrestrial or aerological branches of the hydrological cycle ([Gilman and Garrett 1994](#)). For the terrestrial analysis, the net evaporation is given by the sum of river runoff into the basin and the freshwater flux through the Strait of Gibraltar, while for the aerological analysis it is equated with the divergence of the vertically integrated horizontal water vapor flux. [Gilman and Garrett \(1994\)](#) quote values of $E - P = 0.78$ and 0.66 m yr^{-1} from the terrestrial and aerological branches, respectively. Estimates may also be obtained from bulk formulas, although

these are sensitive to the choice of parameterizations used to calculate evaporation. A recent analysis from the Southampton Oceanography Centre (SOC) ([Josey et al. 1999](#)), based on the Comprehensive Ocean–Atmosphere Data Set (COADS) data, gives a basin averaged $E - P$ of 0.71 m yr^{-1} , between the aerological and terrestrial estimates discussed above. [Artegianni et al. \(1997\)](#) suggest a freshwater gain for the Adriatic of 1.14 m yr^{-1} , but suspect the precipitation budget may be significantly overestimated due to a lack of open ocean measurements and a coastal bias, possibly by up to 50%. Although the Adriatic must have a net surface freshwater gain, a lower precipitation would leave the aerological component of the flux [$E - P$, ignoring runoff (R)] comparable to 0.51 m yr^{-1} of net evaporation found by ([Josey et al. 1999](#)) for this basin.

b. Modeled fluxes

From the last 15 years of the restoring integration, the surface fluxes of heat and freshwater are diagnosed from the boundary conditions [[Eqs. \(1\) and \(2\)](#)] and used to calculate basin averages. Fluxes are calculated every time step and accumulated to be output as monthly averages, from which annual averages are found ([Fig. 2](#)). The monthly basin averaged values, as well as averages over four subregions for each experiment, are listed in [Table 1](#). Note that since fluxes are derived from observed temperature and salinity values, runoff (R) signature from rivers, and the Bosphorus are implicitly included.

The diagnosed basin-averaged heat flux falls well within the observational estimates. The heat loss is concentrated in several regions, associated with convection in the northern basin or Ekman downwelling along the African coasts ([Fig. 2a](#)), although the scales of these fluxes are undoubtedly too small. The large-scale net excess evaporation also agrees with observations. Largest excess evaporation is concentrated along the path of the incoming modified Atlantic water (MAW), in the Alboran, the Ionian, and along the path of the mid-Mediterranean jet (MMJ) across the eastern basin ([Fig. 2b](#)). The model has slightly more heat loss per unit area in the western basin than in the eastern basin. Excess evaporation is also higher in the western basin, with the largest contribution associated with the modification of the incoming fresh Atlantic water. The biggest discrepancy with the observational estimates is in the Adriatic, where the heat loss is about twice that suggested by [Artegianni et al. \(1997\)](#) and the modeled “precipitation” is significantly less. However, the Adriatic shows a net surface buoyancy loss, as expected, and the observational estimates have known biases which may account for the differences.

There is a strong seasonal cycle associated with both components of the surface buoyancy flux, especially for heat ([Table 1](#)). The larger western basin heat loss is mainly due to winter convection in the Gulf of Lions. The significant drop in excess evaporation in spring might be realistically related to extra runoff, which is implicitly included through lower surface salinities in the restoring boundary conditions. We calculated the seasonal heat fluxes over the Mediterranean from the SOC climatology ([Josey et al. 1999](#)) and find our seasonal cycle in heat fluxes to be in phase with those from the climatology but smaller in amplitude by a factor of about 2. The amplitude is also smaller (by about $\frac{1}{3}$) than that found in a modeling study by [Haines and Wu \(1998\)](#), although the annual mean is about the same, showing that the seasonal cycle can be model dependent. The weak seasonal cycle in heat flux is probably related to the lack of vertical diffusion near the surface due to using the GM mixing scheme which leads to a very shallow summer mixed layer. Thus, not enough heat is added to the basin in the summer while not enough is lost in the winter. To improve this would require improvement of the behavior of GM near the surface, which is beyond the scope of this paper.

4. Model behavior under flux forcing

The monthly averaged fluxes described in [section 3b](#) were used to directly force the model, with the actual fluxes at any given time step determined by linear interpolation. Although this process can lead to differences in the monthly means from the original diagnosed forcing ([Killworth 1996](#)), in almost all months the differences are small (especially for the heat flux) and the resulting annual mean is the same as that of the diagnosed fluxes.

Other than in the Gibraltar box (parameterizing the Atlantic inflow) all restoring boundary conditions were removed. Otherwise, the model and the numerical parameters remained the same. Initial conditions were taken from the end of the 100-yr relaxation run and the model was forced for another 100 years with the flux boundary conditions.

Surprisingly, on switching to the surface flux boundary conditions, the model remained stable, with little change in its basic state, circulation patterns, or water masses. A time series of the kinetic energy density, [Fig. 3](#), shows that the model has remained stable, despite the change in forcing. The switch to flux boundary conditions leads to a very slight increase in the amplitude of the seasonal cycle for the basin-averaged kinetic energy density, by about 3%. The original surface relaxation was not therefore inhibiting the energetics of the model significantly. Over the 100 years of flux-forced integration, the basin-averaged temperature decreased by less than 0.05°C and the basin-averaged salinity increased by less than 0.02 psu. Both of these changes occurred within the first 50 years after the switch in boundary conditions.

Snapshots of the basin’s surface summer and wintertime circulation from the free surface height are shown in [Fig. 4](#).

Although limited by the $\frac{1}{4}^\circ$ resolution, significant structure and seasonal variability can be seen in the Alboran Sea and Algerian Current. The Asia Minor current is strong in winter and weak in summer, as is the Rhodes gyre. The seasonal Shikmona gyre appears off the Israeli coast only in summer.

That a steady state has been reached can be seen from the transports of heat and salt through the Straits of Gibraltar, Sicily, and Otranto. [Table 2](#) shows the transports through the main straits of the basin. Gibraltar volume transport is higher than many recent estimates (cf. [Herbaut et al. 1997](#)), with the main reason probably being the large cross-sectional area of the model strait, double the real strait (related to our $\frac{1}{4}^\circ$ resolution and rectangular cross section). The use of the Gent and McWilliams parameterization and the flux limiter also increases the Gibraltar volume transport, by about 0.2 Sv ($\text{Sv} \equiv 10^6 \text{ m}^3 \text{ s}^{-1}$). The heat transport through Gibraltar is equivalent to a heat gain of 6.0 W m^{-2} spread over the surface area of the basin, balancing the surface heat loss of 6.1 W m^{-2} ([Table 1](#)). The input of freshwater to the basin is equivalent to a net precipitation over the surface of 0.78 m yr^{-1} , again balancing the surface fluxes. Similar agreements can be found for the eastern basin and the Adriatic separately. No such balance is to be found seasonally. The Gibraltar and Sicily freshwater fluxes show only a weak seasonal cycle and the heat fluxes are out of phase with the surface fluxes, with less heat being exchanged at the straits in winter. The transports of heat and freshwater at the Strait of Sicily ([Table 2](#)) suggest a minimum LIW transport in winter and spring and a maximum through summer and autumn, consistent with the findings of [Manzella and La Violette \(1990\)](#).

An additional experiment was performed with the surface fluxes averaged onto a $1^\circ \times 1^\circ$ grid before being used to force the model. A 40-yr integration produced similar results (currents and water masses, with no property difference larger than 0.1 psu and 0.2°C below the top 200 m) to those obtained with the unsmoothed fluxes in [Fig. 2](#). The significance of the fact that the model is able to run and remain stable with these coarser scale fluxes is that most observational climatologies (or products of numerical weather prediction models) exist mainly at coarser scales.

a. Water properties: Transformations and pathways

A number of well-defined major water masses are formed in the Mediterranean: Levantine Intermediate Water, Cretan Intermediate Water (CIW), Western Mediterranean Deep Water, and Eastern Mediterranean Deep Water. Although recent changes (since 1987) to some of these waters have been observed by [Roether et al. \(1996\)](#), the modeled mean production of all these water masses is reasonably similar to the pre-1987 state in terms of source regions, amount of production, and T and S properties and distribution. However, under flux boundary conditions there is more variability in water formation.

Observations suggest a wide density range for LIW ($\sigma_\theta = 28.93\text{--}29.11$) with the single isopycnal ($\sigma_\theta = 29.05$) possibly representative of the spreading core of the water mass in the eastern basin ([Roether et al. 1998](#)). The model's core LIW ($\sigma_\theta = 29.04\text{--}29.10$) is formed in the Rhodes gyre and in a small region in the south Cretan Sea, with convection occurring to depths between 200 and 350 m. Shallower convection, forming water at the lighter end of the LIW range, occurs over much of the lower Aegean and northern Levantine. By examining the change in water volume in the Levantine between the $\sigma_\theta = 28.93\text{--}29.11$ isopycnals and the export from the Levantine over the course of the winter, one finds the total annual-average production of LIW in the model to be 1.3 Sv with significant interannual variability.

Following [Tziperman and Speer \(1994\)](#), the instantaneous cross-isopycnal volume flux due to buoyancy forcing in the surface layer, $F(\rho')$, is given by

$$F(\rho') = \frac{1}{\rho_o} \iint_A dA \left[\frac{\alpha}{C_p} \mathcal{H}(x, y, t) - \rho\beta S(x, y, t) Q(x, y, t) \right] \times \delta[\rho(x, y, t) - \rho'], \quad (3)$$

where $\mathcal{H}(x, y, t)$ and $Q(x, y, t)$ are the surface fluxes of heat and freshwater, respectively, and where the fluxes penetrate only the top 10-m layer of the ocean (the thickness of the top model layer); C_p is the specific heat capacity of water while α and β are the derivatives of density with respect to temperature and salinity, respectively; $S(x, y, t)$ is the surface salinity and $\rho(x, y, t)$ is the surface density. Integrating over 100 years, the average surface water mass conversion of lighter water to LIW ($\sigma_\theta = 28.93\text{--}29.11$) is 1.2 Sv east of 25.5°E in the Levantine Basin. Estimates of LIW production range from 1.0 Sv by [Lascaratos et al. \(1993\)](#) to 1.5 Sv by [Tziperman and Speer \(1994\)](#).

The surface production is balanced by LIW export, either by advection to the rest of the basin or by diapycnal mixing processes to other density classes. Transformation of more dense waters into this class produces another 0.1 Sv balancing

the 0.1 Sv of deep inflow in the Levantine below the LIW layer. Direct advection to the west, around 25.5°E, within the $\sigma_\theta = 28.93\text{--}29.11$ range, is 0.6 Sv. The remaining 0.7 Sv is converted to density classes lighter than $\sigma_\theta = 28.93$, with 0.2 Sv of this being exported westward in the $\sigma_\theta = 28.85\text{--}28.93$ range. An overview of the model LIW budget in the Levantine is presented schematically in [Fig. 5](#), including the interannual standard deviations. Although holding on the long-term average, this balance does not necessarily hold each year as changes in volume can allow for the production to exceed the export/conversion in some years with the reverse holding in other years, as discussed in [section 4b](#).

The average seasonal variations have surface production in this LIW density class limited to 3 months in winter during isopycnal outcropping. Following convection and water formation, the mixing to lower density classes and advective export both peak in March and decay slowly through the rest of the year to the following winter, [Fig. 6](#). Upwelling from below remains basically constant throughout the year. All told, this leads to mean seasonal variations in the LIW volume within the Levantine of $1.5 \times 10^{13} \text{ m}^3$, with a maximum volume in March of $\sim 3.5 \times 10^{13} \text{ m}^3$.

On the core $\sigma_\theta = 29.05$ isopycnal, the salinities are in the low end of the observed range while the temperatures are also slightly low [Fig. 7](#) ([Lascaratos et al. 1993](#); [Roether et al. 1998](#)). The dispersal pathways from the Levantine are largely consistent with [Fig. 4](#) of [Roether et al. \(1998\)](#), with the main pathway to the west being through the south/central Ionian with a northern path along the Greek coast towards the Adriatic. LIW dispersal is sensitive to the path of the MMJ, as shown by [Myers et al. \(1998a\)](#). When the MMJ is farther south, there is significant westward LIW transport south of Crete. This decreases and occurs at a deeper depth (with more transport to the north of Crete) when the MMJ occupies a more northerly position.

In the northern Cretan Sea and the lower Aegean, CIW is formed, sinking to depths of 300–400 m initially. Then, upon leaving the Aegean, it descends farther to a 500–1000-m range. Surface production [calculated using [Eq. \(3\)](#)] of this water mass with density $\sigma_\theta = 29.15\text{--}29.22$ ([El-Gindy and El-Din 1986](#)), is fairly small, being only 0.1–0.2 Sv in the model. The model CIW has a salinity of 38.8–39.0 psu and a potential temperature of 13.9°–14.5°C ([Fig. 7](#)). The CIW spreads from the Aegean, as a high salinity tongue, mainly through the Kytheran Strait, on the $\sigma_\theta = 29.15$ isopycnal, into the Ionian.

Observations ([El-Gindy and El-Din 1986](#); [Schlitzer et al. 1991](#)) show CIW occurring between 700 m and 1300 m, with a potential temperature of $\theta = 14.02^\circ\text{--}14.6^\circ\text{C}$ and a salinity of 38.85–39.0 psu. The model spreading pattern resembles that observed, except to the east of Crete where the model outflow through Kassos Strait is too fresh and weak.

In winter, cold temperatures combined with salty intermediate water (LIW) leads to a complete overturning of the lower Adriatic. From December to March the mean volume of water with density greater than $\sigma_\theta = 29.0$ in the Adriatic increases by 0.6–0.7 ($\times 10^{13} \text{ m}^3$). A calculation using [Eq. \(3\)](#) shows that this water formation process is almost entirely surface generated. Adriatic deep water then overflows the sill at the Strait of Otranto to sink and fill the deep eastern basin as EMDW, [Fig. 8a](#). Salinities range from 38.4 psu in the Adriatic to 38.65 psu in the deep Ionian and potential temperatures similarly range from 12.0° to 13.2°C ([Fig. 7](#)). After leaving the Adriatic, the model EMDW sinks to $\sigma_\theta = 29.22$ and flows southward in a western boundary undercurrent, which then feeds the interior of the Ionian and parts of the Levantine.

In the west, cold winter winds associated with the mistral blowing off the coast of France lead to vigorous surface cooling in the Gulf of Lions. In the model reduced stratification due to the presence of subsurface LIW and the spinup of a strong cyclonic circulation in the region, means convection penetrates to the bottom ([Fig. 8b](#)), consistent with numerous field studies ([Gascard 1978](#); [Lacombe et al. 1981](#); [Thetis Group 1994](#)). The model produces deep convection to at least 2000 m in most years with an annually averaged production of water with density greater than $\sigma_\theta = 29.0$ of 0.2–0.3 Sv.

[Equation \(3\)](#) shows that around 70%–75% of the buoyancy forcing for the water mass conversion comes from the wintertime heat loss. The water in the convection region normally reaches a density of $\sigma_\theta = 29.13$ with a salinity of around 38.38 psu and a potential temperature of $\theta = 12.4^\circ\text{C}$ ([Fig. 7](#)). Deep model currents and properties on the $\sigma_\theta = 29.13$ isopycnal show that this deep water flows cyclonically southward along the shelfbreak off the Spanish coast and Balearic Islands as a deep western boundary current before feeding the interior of the basin. Disorganized flow in the central and eastern part of the basin and eventually providing a weak overflow into the Tyrrhenian.

b. Variability in water formation under flux forcing

[Figure 9](#) shows the LIW ($\sigma_\theta = 28.93\text{--}29.11$) volume change between December and March each year, expressed as a formation rate averaged over a year. The power spectrum, [Fig. 10](#), of this time series reveals that the main periods of variability are in the interannual range (2 yr) and the interdecadal range (12–16 yr). The shorter period variability is associated with changes in the advection pathways for MAW in the Levantine. An observational study of [Oszoy et al. \(1991\)](#) first suggested that shifts in the bifurcation position of the MMJ leads to changes in the transport of MAW to the Rhodes

gyre region. In particular, when MAW is transported along a longer path to the south and east of Cyprus, it spends more time within a zone of higher net evaporation and thus has a higher salinity when it arrives at the LIW formation sites.

The LIW formation rate in the model is most sensitive to the background salinity, with the saltier the water, the more LIW that is able to form. The wintertime surface salinity in the Rhodes gyre (between Crete and Cyprus, north of 33.5°N) varies by up to 0.1 psu between winters and is well correlated with the LIW volume formed (Fig. 9), with $r = 0.85$. Note that in this and all subsequent calculations of correlations, the first 10 years of the flux experiment are discarded.

Variations in the LIW volume each year (Fig. 9) feed back on the MMJ and its path in the following year. In all years, the MMJ bifurcates to the east of the Mersah–Matruh gyre. In some years, the northward branch flows to the west of Cyprus in a broad deep current (~150 km wide and 180 m deep), with little input from the southern branch along the African shore, which instead flows north to the east of Cyprus, feeding the Asia Minor current. A composite of 60-m currents in such years is shown in Fig. 11a. In fact, Fig. 11a is a composite of all years with an annual equivalent LIW production less than 1.1 Sv, according to Fig. 9, and Fig. 11b shows all years with LIW production >1.7 Sv.

The end result of the current pattern in Fig. 11a is less evaporation and a lower salinity for the MAW entering the Rhodes gyre. This leads to a decrease in the volume of LIW produced the following winter with convection mainly occurring in the eastern Rhodes gyre and to shallower depths in the northern Levantine approaching Cyprus. Surface salinity is not high enough in the western Rhodes gyre to allow for significant convection there. With LIW formation occurring in the central/eastern parts of the Rhodes gyre, there is more dispersal toward the east Levantine and Cyprus and a longer residence time inside the Levantine Basin.

In the following year the presence of LIW to the west of Cyprus partially blocks the deep flow of MAW to this region by the northern branch of the MMJ, leading to currents like those in Fig. 11b. The southern MAW pathway along the African coast is then the dominant pathway leading to significant extra evaporation, a higher wintertime salinity in the Rhodes gyre, and more LIW production in the following year. After these high LIW production winters the majority of the LIW is entrained into the deep westward current flowing to the south of Crete, with a shorter LIW residence time inside the Levantine. The northern branch of the MMJ therefore broadens and deepens again, allowing significant amounts of fresher MAW into the Rhodes gyre region, and the cycle repeats. The difference in freshwater transport (across a zonal section to the west of Cyprus) into the northern Levantine and Rhodes gyre region between low and high LIW production years (as defined previously) differs by about 20% between the two extremes of these different circulation schemes.

Other than one or two large events, the variability of EMDW volume in the Adriatic is smaller than for the LIW (Fig. 9). The power spectrum (Fig. 10b) shows that the dominant period of variability for the EMDW is in the decadal range (15–20 yr and longer), with a weaker peak around 2 yr. The LIW and EMDW time series have a maximum correlation of $r = 0.62$ at a lag of 2 yr (LIW leading EMDW), significant at the 95% level. Wu and Haines (1996) suggest some newly formed LIW can reach the Adriatic within 1 yr, while Stratford and Williams (1997) suggest 3–5 yr is the average timescale. The power spectra of the transports of mass, heat, and freshwater through the Otranto Strait also show peaks at a frequency of 2 yr. The freshwater transport into the Adriatic and the EMDW formation show a negative correlation of $r = 0.48$ at a lag of –3 months (freshwater transport precedes reduced EMDW formation by 3 months). Variations in LIW production leads to changes in the import to the Adriatic and thus the salt available for preconditioning the water column for EMDW formation. The variability in WMDW production (not shown) is also correlated with the LIW production, $r = 0.59$, at a lag of 6 yr. These results show the importance of LIW as a preconditioning agent for the formation of deep waters across the Mediterranean.

5. Discussion and summary

A 200-yr integration of a numerical model of the Mediterranean has been carried out. An initial 100-yr integration under surface T , S restoring boundary conditions showed that the model successfully simulated the circulation and water masses of the basin. The diagnosed surface fluxes of heat and freshwater are quite realistic on the annual-average basin scale but have a decreased amplitude seasonal cycle as well as considerable small-scale variability. These fluxes were used to force the model for a further 100 years, with the surface restoring boundary conditions completely removed. The circulation remained stable under the flux forcing, with little (less than 0.05°C and 0.02 psu) drift in water properties and no change in the mean thermohaline circulation.

A water-mass budget analysis showed around 1.2 Sv of LIW ($\sigma_\theta = 28.93$ –29.11) is produced annually at the surface in the Levantine, with another 0.1 Sv formed by diapycnal mixing from denser waters below. This is balanced by a direct export of 0.6 Sv westward to the rest of the basin and a further loss of 0.7 Sv upward by diapycnal mixing processes (Fig. 5) with 0.2 Sv of this lighter water exported in the $\sigma_\theta = 28.85$ –28.93 range. The surface conversion occurs only in late winter, while the other processes carry on year round, albeit with maximum transports and mixing just after the end of convection.

With the flux surface boundary conditions the internal interannual frequency variability is enhanced. The production of LIW varies considerably in a biennial cycle, related to changes in the surface salinity, shifts in the path of the MMJ and the advection of MAW through the Levantine. LIW variability leads changes in EMDW production by 2 years. This connection highlights how the different aspects of the circulation feedback on one another and why explanations of physical processes cannot treat circulation features as independent. For example, while the MMJ is a wind-driven current, some aspects of its path are controlled by the thermohaline forcing from the underlying LIW.

The significance of this study is that it is the first modeling work to produce a detailed and realistic picture of the Mediterranean water masses and thermohaline circulation using flux forcing. Previous attempts to use flux forcing have all been limited by deficiencies in some aspects of the circulation or water masses, or by short integrations. While realistic circulations have been obtained using restoring boundary conditions (e.g., [Wu and Haines 1998](#)), the ability to look at variability in the system is severely limited. With flux boundary conditions the surface water properties are not specified, allowing for more realistic development of different circulation regimes, both for simulating ongoing and future changes (e.g., [Roether et al. 1996](#)), or for better simulations of past paleoclimates, ([Rohling 1994](#); Myers et al. 1998). For example, ongoing work is studying the possibility of multiple equilibria in the Mediterranean thermohaline circulation (Myers and Haines 2000, manuscript submitted to *Dyn. Atmos. Oceans*).

Acknowledgments

We would like to thank Peili Wu, Kevin Stratford, Ric Williams, Simon Josey, and other members of the CLIVAMP and MATER project groups for helpful discussions. This work was funded by the EU MAST CLIVAMP program under Contract MAS3-CT95-0043.

REFERENCES

- Artegiani, A., D. Bregant, E. Paschini, N. Pinardi, F. Raicich, and A. Russo, 1997: The Adriatic Sea general circulation. Part I: Air-sea interactions and water mass structure. *J. Phys. Oceanogr.*, **27**, 1492–1514.. [Find this article online](#)
- Barnier, B., L. Siefridt, and P. Marchesiello, 1995: Thermal forcing for a global-ocean circulation model using a three-year climatology of ECMWF analyses. *J. Mar. Syst.*, **6**, 363–380..
- Beckers, J. M., and Coauthors, 1996: First annual report: Mediterranean model evaluation experiment MEDMEX, E.U. concerted action. Tech. Rep. 1, 32 pp. [Available from Communication Unit, European Commission, SDME 2185, Wetstraat, 200 Rue de la Loi, B-1049 Brussels, Belgium.].
- , and Coauthors, 1997: Second annual report: Mediterranean models evaluation experiment MEDMEX, E.U. concerted action. Tech. Rep. 2, 34 pp. [Available from Communication Unit, European Commission, SDME 2185, Wetstraat, 200 Rue de la Loi, B-1049 Brussels, Belgium.].
- Bethoux, J. P., 1979: Budgets of the Mediterranean Sea. Their dependence on the local climate and on characteristics of the Atlantic waters. *Oceanol. Acta*, **2**, 157–163..
- Brasseur, P., J. M. Beckers, J. M. Brankart, and R. Schoenauen, 1996: Seasonal temperature and salinity fields in the Mediterranean Sea: Climatological analyses of a historical data set. *Deep-Sea Res.*, **43**, 159–192..
- El-Gindy, A. A. H., and S. H. S. El-Din, 1986: Water masses and circulation patterns in the deep layer of the Eastern Mediterranean. *Oceanol. Acta*, **9**, 239–248..
- Gascard, J., 1978: Mediterranean deep water formation, baroclinic instability and oceanic eddies. *Oceanol. Acta*, **1**, 315–330..
- Gent, P. R., and J. C. McWilliams, 1990: Isopycnal mixing in ocean circulation models. *J. Phys. Oceanogr.*, **20**, 150–155.. [Find this article online](#)
- Gilman, C., and C. Garrett, 1994: Heat flux parameterizations for the Mediterranean Sea: The role of atmospheric aerosols and constraints from the water budget. *J. Geophys. Res.*, **99**, 5119–5134..
- Haines, K., and P. Wu, 1995: A modelling study of the thermohaline circulation of the Mediterranean Sea: Water formation and dispersal. *Oceanol. Acta*, **18**, 401–417..
- , and —, 1998: GCM studies of intermediate and deep waters in the Mediterranean. *J. Mar. Syst.*, **18**, 197–214..
- Haney, R. S., 1971: Surface thermal boundary conditions for ocean circulation models. *J. Phys. Oceanogr.*, **1**, 241–248.. [Find this article](#)

Herbaut, C., L. Mortier, and M. Crepon, 1996: A sensitivity study of the general circulation of the Western Mediterranean Sea. Part I: The response to density forcing through the straits. *J. Phys. Oceanogr.*, **26**, 65–84.. [Find this article online](#)

—, F. Martel, and M. Crepon, 1997: A sensitivity study of the general circulation of the Western Mediterranean Sea. Part II: The response to atmospheric forcing. *J. Phys. Oceanogr.*, **27**, 2126–2145.. [Find this article online](#)

Jaeger, L., 1976: Monatskarte des niederschlags für die ganze Erde. Tech. Rep. 18, Ber. Dtsch. Wetterdienstes, 39 pp..

Josey, S., E. Kent, and P. Taylor, 1999: New insights into the ocean heat budget closure problem from analysis of the SOC air–sea flux climatology. *J. Climate*, **12**, 2856–2880.. [Find this article online](#)

Killworth, P., 1996: Time interpolation of forcing fields in ocean models. *J. Phys. Oceanogr.*, **26**, 136–143.. [Find this article online](#)

—, D. Stainforth, D. J. Webb, and S. M. Paterson, 1991: The development of a free-surface Bryan–Cox–Semtner ocean model. *J. Phys. Oceanogr.*, **21**, 1333–1348.. [Find this article online](#)

Kinder, T. H., and G. Parrilla, 1987: Yes, some of the Mediterranean outflow does come from great depth. *J. Geophys. Res.*, **92**, 2901–2906..

Lacombe, H., J. Gascard, J. Gonella, and J. Bethoux, 1981: Response of the Mediterranean to the water and energy fluxes across its surface, on seasonal and interannual scales. *Oceanol. Acta*, **4**, 247–255..

Lascaratos, A., R. G. Williams, and E. Tragou, 1993: A mixed-layer study of the formation of Levantine Intermediate Water. *J. Geophys. Res.*, **98**, 14 739–14 749..

Levitus, S., 1982: *Climatological Atlas of the World Ocean*. NOAA Prof. Paper No. 13, U.S. Govt. Printing Office, 173 pp..

Macdonald, A., J. Candela, and H. L. Bryden, 1994: An estimate of the net heat transport through the Strait of Gibraltar. *Seasonal and Interannual Variability of the Western Mediterranean Sea*, P. E. La Violette, Ed., *Coastal Estuarine Studies*, Vol. 46, Amer. Geophys. Union, 13–32..

Manabe, S., and R. J. Stouffer, 1988: Two stable equilibria of a coupled ocean–atmosphere model. *J. Climate*, **1**, 841–866.. [Find this article online](#)

Manzella, G. M. R., and P. E. La Violette, 1990: The seasonal variation of water mass content in the western Mediterranean and its relationship with the inflows through the straits of Gibraltar and Sicily. *J. Geophys. Res.*, **95**, 1623–1626..

May, P. W., 1982: Climatological flux estimates in the Mediterranean Sea: Part I. Winds and wind stresses. Tech. Rep. 54, NORDA..

Myers, P. G., K. Haines, and S. Josey, 1998a: On the importance of the choice of wind stress forcing to the modelling of the Mediterranean Sea circulation. *J. Geophys. Res.*, **103**, 15 729–15 749..

—, —, and E. J. Rohling, 1998b: Modelling the paleo-circulation of the Mediterranean: The last glacial maximum and the Holocene with emphasis on the formation of Sapropel S_1 . *Paleoceanography*, **13**, 586–606..

Ozsoy, E., A. Hecht, U. Unluata, S. Brenner, T. Oguz, J. Bishop, M. A. Latif, and Z. Rozenraub, 1991: A review of the Levantine Basin circulation and its variability during 1985–1988. *Dyn. Atmos. Oceans*, **15**, 421–456..

Pinardi, N., and A. Navarra, 1993: Baroclinic wind adjustment processes in the Mediterranean Sea. *Deep Sea Res.*, **40**, 1299–1326..

Rahmstorf, S., 1993: A fast and complete convection scheme for ocean models. *Ocean Modelling* (unpublished manuscripts), **101**, 9–11..

Robinson, M. K., R. A. Bauer, and E. H. Schroeder, 1971: Atlas of North Atlantic–Indian Ocean monthly mean temperatures and mean salinities of the surface layer. Tech. Rep. 18, Naval Office of Reference Publication..

Roether, W., B. B. Manca, B. Klein, D. Bregant, D. Georgopoulos, V. Beitzel, V. Kovacevic, and A. Luchetta, 1996: Recent changes in eastern Mediterranean deep waters. *Science*, **271**, 333–335..

—, B. Klein, V. Beitzel, and B. Manca, 1998: Property distributions and transient-tracer ages in the Levantine Intermediate Water in the eastern Mediterranean. *J. Mar. Syst.*, **18**, 71–87..

Rohling, E. J., 1994: Review and new aspects concerning the formation of eastern Mediterranean sapropels. *Mar. Geol.*, **122**, 1–28..

Roussenov, V., E. Stanev, V. Artale, and N. Pinardi, 1995: A seasonal model of the Mediterranean Sea general circulation. *J. Geophys. Res.*,

Schlitzer, R., W. Roether, H. Oster, H.-G. Junghans, M. Hausmann, H. Johansen, and A. Michelato, 1991: Chlorofluoromethane and oxygen in the eastern Mediterranean. *Deep-Sea Res.*, **38**, 1531–1551..

Send, U., G. Krahnmann, and C. Millot, 1997: Acoustic observations of heat content across the Mediterranean Sea. *Nature*, **385**, 615–618..

Stanev, E. V., J. J. Friedrich, and S. V. Botev, 1989: On the seasonal response of intermediate and deep water to surface forcing in the Mediterranean Sea. *Oceanol. Acta*, **12**, 141–149..

Stratford, K., 1999: Flux-limited advection for tracers in an ocean general circulation model. *J. Atmos. Oceanic Technol.*, **16**, 1284–1290..

—, and R. G. Williams, 1997: A tracer study of the formation, dispersal and renewal of Levantine Intermediate Water. *J. Geophys. Res.*, **102**, 539–549..

Thetis Group, 1994: Open-ocean deep convection explored in the Mediterranean. *Eos, Trans. Amer. Geophys. Union*, **75**, 219–221..

Thuburn, J., 1996: Multidimensional flux-limited advection schemes. *J. Comput. Phys.*, **123**, 74–83..

Tziperman, E., and K. Speer, 1994: A study of water mass transformation in the Mediterranean Sea: Analysis of climatological data and a simple three-box model. *Dyn. Atmos. Oceans*, **21**, 53–82..

Weaver, A. J., and T. M. C. Hughes, 1992: Stability and variability of the thermohaline circulation and its link to climate. *Trends Phys. Oceanogr.*, **1**, 15–70..

Webb, D. J., 1993: An ocean model code for array processor computers. Tech. Rep. 324. Institute of Oceanographic Sciences, Wormley, United Kingdom, 8 pp. [Available from Southampton Oceanography Centre, Southampton SO14 3ZH, United Kingdom.].

—, 1995: The vertical advection of modelling in Bryan–Cox–Semtner ocean general circulation models. *J. Phys. Oceanogr.*, **25**, 3186–3195.. [Find this article online](#)

Wu, P., and K. Haines, 1996: Modelling the dispersal of Levantine Intermediate Water and its role in Mediterranean deep water formation. *J. Geophys. Res.*, **101**, 6591–6607..

—, and —, 1998: The general circulation of the Mediterranean Sea from a 100-year simulation. *J. Geophys. Res.*, **103**, 1121–1135..

Zavatarelli, M., and G. L. Mellor, 1995: A numerical study of the Mediterranean Sea circulation. *J. Phys. Oceanogr.*, **25**, 1384–1414.. [Find this article online](#)

Tables

Table 1. Surface heat ($W m^{-2}$) and freshwater fluxes ($cm yr^{-1}$) diagnosed from the final 15 years of the model spinup under restoring boundary conditions, for both the annual and monthly averages. The regional abbreviations are MED: basin average, WMED: the Western Mediterranean, EMED: the Eastern Mediterranean (including the Adriatic and Aegean), AD: the Adriatic, and AG: the Aegean to the north of 36° .

Period	Heat flux ($W m^{-2}$)					$E - P - R$ ($cm yr^{-1}$)				
	MED	WMED	EMED	AD	AG	MED	WMED	EMED	AD	AG
Annual mean	-6.1	-7.3	-5.1	-41	-27	76	94	66	-20	-34
Jan	-81	-111	-66	-138	-169	180	255	157	-19	63
Feb	-72	-73	-71	-104	-99	207	176	285	-82	235
Mar	-3.0	0.5	-4.5	1.7	-23	97	151	69	-27	16
Apr	27	30	26	32	20	21	55	3.4	-63	-67
May	53	49	56	47	62	-31	-1.8	-46	-107	-207
Jun	66	63	68	48	66	-61.1	18	-10	-30	-60
Jul	48	48	49	31	35	29	23	32	20	-61
Aug	19	18	21	-210	17	37	50	30	21	-101
Sep	-6.9	-1.7	-9.2	-28	-11	22	31	17	61	-120
Oct	-26	-20	-29	-58	-36	31	30	32	18	-66
Nov	-40	-28	-46	-58	-85	99	115	98	-46	46
Dec	-57	-62	-54	-81	-112	178	252	139	13	32

Click on thumbnail for full-sized image.

Table 2. Volume, heat, and equivalent freshwater transports through each of the Straits of Gibraltar, Sicily, and Otranto with annual and seasonal averages from the final 15 years of the flux forced integration. The sign convention for the heat and freshwater transports is that a positive value indicates transport into the basin and negative is a transport out (Mediterranean, Eastern Mediterranean, and Adriatic, respectively). The seasons are defined as summer: JAS, autumn:OND; winter: JFM, and spring: AMJ.

--

Sicily	annual	1.09	14.51	0.027
	summer	1.07	14.56	0.027
	autumn	1.21	9.95	0.038
	winter	0.93	1.74	0.031
	spring	0.85	4.42	0.029
Otranto	annual	0.47	3.76	-0.0008
	summer	0.35	4.56	-0.0002
	autumn	0.27	2.24	0.0006
	winter	0.82	4.91	-0.0017
	spring	0.42	3.34	-0.0016

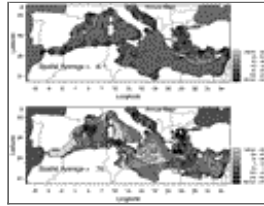
[Click on thumbnail for full-sized image.](#)

Figures



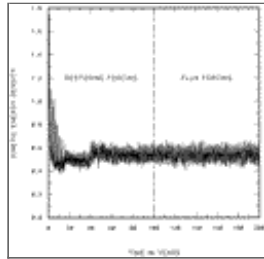
[Click on thumbnail for full-sized image.](#)

Fig. 1. A map detailing some of the main Mediterranean locations mentioned in this paper.



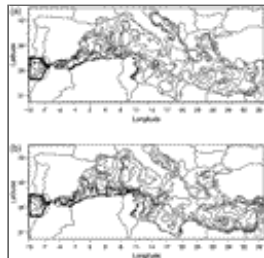
[Click on thumbnail for full-sized image.](#)

Fig. 2. Annual average of surface fluxes of (a) heat ($W m^{-2}$) and (b) freshwater ($cm yr^{-1}$) averaged over the last 15 years of surface restoring integration.



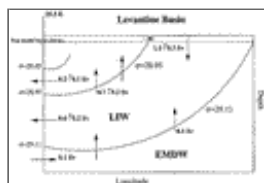
[Click on thumbnail for full-sized image.](#)

Fig. 3. Basin averaged kinetic energy density ($kg m^{-1} s^{-2}$) over the period of integration. At 40 years the GM parameter was decreased, and at year 100 the switch from restoring to flux surface boundary conditions occurred, marked by the broken vertical line.



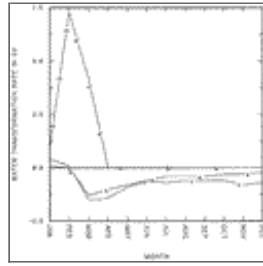
[Click on thumbnail for full-sized image.](#)

Fig. 4. Snapshots of the basin's free surface height, showing the surface circulation for (a) Jun and (b) Dec. The contour interval is 3.0 cm.



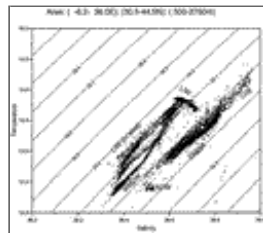
[Click on thumbnail for full-sized image.](#)

Fig. 5. Schematic of model processes and transports, annually averaged, involving LIW in the Levantine east of 25.5°E. The range in the values indicates the first standard deviation of the interannual variability.



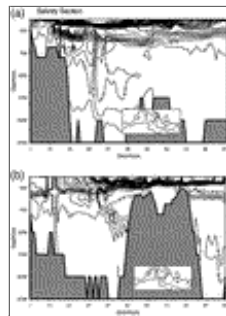
[Click on thumbnail for full-sized image.](#)

Fig. 6. Mean seasonal cycle of the water mass transformations involving LIW in the Levantine. Shown are the volume transport across 25.5°E (line a), the surface formation (line b), and the conversion across the $\sigma_\theta = 28.93$ isopycnal (line c). The conversion across the $\sigma_\theta = 29.11$ isopycnal is not shown as it remains essentially constant at 0.1 Sv. A positive transformation is associated with a transfer into the LIW layer, and negative out.



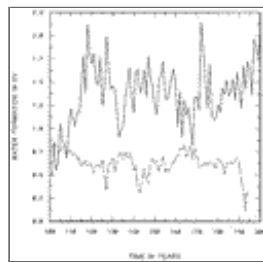
[Click on thumbnail for full-sized image.](#)

Fig. 7. A $T-S$ scatterplot showing some of the main water masses below 500 m in the final year of the model integration. See text for the definitions of the abbreviations.



[Click on thumbnail for full-sized image.](#)

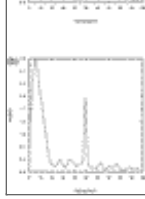
Fig. 8. Model transects for (a) annually averaged salinity through the Eastern Mediterranean and Adriatic for the final year of integration and (b) late wintertime (March) salinity for year 199 through the Strait of Sicily, Western Mediterranean and Gulf of Lions. Paths are shown inset. The contour intervals are 0.025 psu in (a) and 0.05 psu in (b).



[Click on thumbnail for full-sized image.](#)

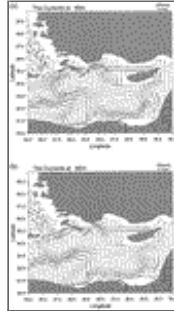
Fig. 9. Time series of the annual equivalent formation rate of LIW in the Levantine (solid line), $\sigma_\theta = 28.93-29.11$, and EMDW in the Adriatic (dashed line), $\sigma_\theta > 29.0$, from each winter (in Sv) over the 100 years of the flux forced integration.





[Click on thumbnail for full-sized image.](#)

Fig. 10. Power spectral density (in Sv^2) of the time series portrayed in [Fig. 9](#) for (a) LIW and (b) EMDW. The x axis corresponds to the number of cycles over the 100 years of the flux forced integration.



[Click on thumbnail for full-sized image.](#)

Fig. 11. Plots of model currents at 60 m in the Levantine during Jun, from composites of all years with (a) strong LIW formation the previous winter and significant MAW transport to the west of Cyprus, and (b) weak LIW formation the previous winter with little MAW transport to the west of Cyprus. Definitions of strong and weak years are given in the text.

Corresponding author address: Dr. Paul G. Myers, Dept. of Physics and Physical Oceanography, Memorial University of Newfoundland, St. John's, Newfoundland A1B 3X7, Canada.

E-mail: paulm@met.ed.ac.uk

[top](#) ▲



© 2008 American Meteorological Society [Privacy Policy and Disclaimer](#)
Headquarters: 45 Beacon Street Boston, MA 02108-3693
DC Office: 1120 G Street, NW, Suite 800 Washington DC, 20005-3826
amsinfo@ametsoc.org Phone: 617-227-2425 Fax: 617-742-8718
[Allen Press, Inc.](#) assists in the online publication of AMS journals.